The BCL-2 family member BID plays a role during embryonic development in addition to its BH3-only protein function by acting in parallel to BAX, BAK and BOK

Francine S Ke[1,2], Steven Holloway[1], Rachel T Uren[1,2], Agnes W Wong[1], Melissa H Little[3,4], Ruth M Kluck[1,2], Anne K Voss[1,2,*,†] & Andreas Strasser[1,2,**,†]

Abstract

The intrinsic apoptosis pathway, regulated by the BCL-2 protein family, is essential for embryonic development. Using mice lacking all known apoptosis effectors, BAX, BAK and BOK, we have previously defined the processes during development that require apoptosis. Rare $Bok^{-/-}Bax^{-/-}Bak^{-/-}$ triple knockout (TKO) mice developed to adulthood and several tissues that were thought to require apoptosis during development appeared normal. This raises the question if all apoptosis had been abolished in the TKO mice or if other BCL-2 family members could act as effectors of apoptosis. Here, we investigated the role of BID, generally considered to link the extrinsic and intrinsic apoptosis pathways, acting as a BH3-only protein initiating apoptosis upstream of BAX and BAK. We found that $Bok^{-/-}Bax^{-/-}Bak^{-/-}Bid^{-/-}$ quadruple knockout (QKO) mice have additional developmental anomalies compared to TKO mice, consistent with a role of BID, not only upstream but also in parallel to BAX, BAK and BOK. Mitochondrial experiments identified a small cytochrome c-releasing activity of full-length BID. Collectively, these findings suggest a new effector role for BID in the intrinsic apoptosis pathway.

Introduction

Apoptosis is a form of programmed cell death (Czabotar *et al*, 2014). It is a normal physiological process that occurs in all multicellular organisms, and is fundamental for maintaining tissue homeostasis, eliminating damaged or diseased cells and sculpting the embryo during development (Vaux & Korsmeyer, 1999; Arya & White, 2015; Voss & Strasser, 2020). Apoptosis can be divided into the intrinsic (also known as the mitochondrial or BCL-2-regulated pathway) and extrinsic pathways (also known as the death receptor pathway), which ultimately converge on the activation of caspases that cleave hundreds of cellular targets, leading to ordered cell demolition (Youle & Strasser, 2008).

The intrinsic apoptotic pathway is regulated by the BCL-2 protein family, which comprises proteins that share one or more of the four BH (BCL-2 homology) domains. BCL-2 family members either promote cell survival (BCL-2, BCL-XL, BCL-W, MCL-1 and A1/BFL-1) or cell death. The latter group can be further classified into the multi-BH domain effectors of apoptosis (BAX, BAK and BOK) that are essential for the execution of apoptosis, and the BH3-only proteins (BID, PUMA, NOXA, BIM, BIK, HRK, BAD and BMF) that initiate apoptosis (Czabotar *et al*, 2014). Under unstressed conditions with ample nutrient supply and growth factors, pro-survival BCL-2 family members bind to and keep BAX and BAK in an inactive state. Depending on the death-inducing stimuli received, the levels of different BH3-only proteins are increased by transcriptional or post-transcriptional processes. The BH3-only proteins bind to and inhibit the pro-survival proteins, thereby releasing their restraint on BAX and BAK. Consequently, the unleashed apoptosis effectors permeabilise the mitochondrial outer membrane (MOM), leading to the release of cytochrome *c* and consequent caspase-9 activation, which in turn proteolytically activates downstream effector caspases (caspase-3, -6 and -7) (Czabotar *et al*, 2014). Some BH3-only proteins, such as truncated BID (tBID), BIM and PUMA, are termed 'activators' as they are also reported to directly bind to and activate BAX or BAK (Ren *et al*, 2010; Singh *et al*, 2019).

1 The Walter and Eliza Hall Institute of Medical Research (WEHI), Melbourne, Vic, Australia
2 Department of Medical Biology, University of Melbourne, Melbourne, Vic, Australia
3 Department of Paediatrics, University of Melbourne, Melbourne, Vic, Australia
4 Murdoch Children's Medical Research Institute, Melbourne, Vic, Australia
  *Corresponding author. Tel: +61 3 9345 2555; E-mail: avoss@wehi.edu.au
  **Corresponding author. Tel: +61 3 9345 2555; E-mail: strasser@wehi.edu.au
  †These authors contributed equally to this work as senior authors

The extrinsic apoptosis pathway is triggered by the activation of membrane-bound death receptors (e.g. FAS, TNFR1) by their cognate ligands (FASL, TNF) (Strasser *et al*, 2009; Kaufmann *et al*, 2012). Following the recruitment of adaptor proteins (e.g. FAS-associated death domain, FADD), pro-caspase-8 becomes activated and in turn proteolytically activates the downstream effector caspases to cause cell death. The intrinsic and extrinsic apoptosis pathways can be linked *via* the BH3-only protein, BID (Wang *et al*, 1996). Upon death receptor-induced apoptosis signalling, BID is cleaved by caspase-8 to yield a C-terminal p15 fragment (tBID) that migrates to the MOM to drive BAX/BAK-dependent MOM permeabilisation (MOMP) (Eskes *et al*, 2000; Billen *et al*, 2008). This connection between the intrinsic and extrinsic pathways is essential for FAS-induced apoptosis in so-called type 2 cells, such as hepatocytes and pancreatic β cells in which tBID-mediated activation of the intrinsic pathway is required to generate sufficient caspase activity for cell killing (Yin *et al*, 1999; Kaufmann *et al*, 2007). Conversely, FAS-induced killing of type-1 cells (mostly lymphoid cells) does not require the above-outlined signal amplification (Scaffidi *et al*, 1998; Jost *et al*, 2009).

BID was first discovered in a λ phage expression library screen as a protein that can bind to both BCL-2 and BAX (Wang *et al*, 1996). It is most abundantly expressed in the kidney, brain, spleen, liver and testis. Mice lacking BID are born at the expected Mendelian frequency with no developmental abnormalities reported. However, hepatocytes of these animals are resistant to FAS-induced apoptosis due to their inability to engage the intrinsic apoptotic pathway (Yin *et al*, 1999; Kaufmann *et al*, 2007; Jost *et al*, 2009).

Studies utilising mouse model systems have uncovered the principal effects and physiological roles of many BCL-2 family members (Ranger *et al*, 2001). Gene-targeted mice lacking all identified apoptosis effectors of the BCL-2 family—BAX, BAK and BOK—have revealed the processes that require apoptosis for normal development (Lindsten *et al*, 2000; Ranger *et al*, 2001; Ke *et al*, 2018). These include digit separation in vertebrates, removal of the vaginal septa, midline fusion of body halves (e.g. the palate, neural tube and body wall closure), elimination of supernumerary neurons and maintaining blood cell homeostasis (Voss & Strasser, 2020). Apoptosis was undetectable in embryos lacking BAX, BAK and BOK. However, the fact that other tissues that ordinarily display developmental apoptosis were normal in mice lacking BAX, BAK and BOK (Ke *et al*, 2018), raised the question if all apoptosis had truly been prevented in these triple knockout mice or if another protein could also act as an effector of apoptosis alongside BAX, BAK and BOK.

Although most BH3-only proteins (e.g. BIM, PUMA) are intrinsically unstructured, BID is found to be structurally similar to multi-BH domain proteins, such as BAX (Chou *et al*, 1999; Suzuki *et al*, 2000) and BCL-XL (Muchmore *et al*, 1996; Billen *et al*, 2008). Moreover, membrane-binding mechanistic studies revealed that both BAX and tBID exhibited similar binding properties, as well as similar NMR structures resembling bacterial toxins (e.g. diphtheria toxin and colicins; García-Sáez *et al*, 2004). We therefore hypothesised that full-length BID may have roles in addition to being the precursor of cleaved BID (cBID; p7 + p15 fragments) from which the p15 fragment can bind to other BCL2 family members via its exposed BH3 domain. For example, BID may participate in the intrinsic apoptotic pathway without being cleaved, in a manner that

resembles the actions of BAX and BAK. To test this hypothesis, we generated $Bok^{-/-}Bax^{-/-}Bak^{-/-}Bid^{-/-}$ quadruple knockout (QKO) animals and compared them to $Bok^{-/-}Bax^{-/-}Bak^{-/-}$ triple knockout (TKO) animals that were described in our earlier work (Ke *et al*, 2018). Due to their inability to execute intrinsic apoptosis, most TKO mice do not survive beyond birth and exhibit multiple developmental abnormalities, including persistent interdigital webs and vaginal septa, failure of midline fusion of the palate, neural tube and body wall, supernumerary neural progenitors and blood cells (Ke *et al*, 2018). If BID functioned solely as a BH3-only protein that exerted its effect upstream of BAX- and BAK-dependent apoptosis, its deletion would have no additional impact on the phenotype of TKO mice. However, if defects worsened (or improved), it would imply that BID may have additional non-BH3-only protein roles in apoptosis, or perhaps even in other processes that impact embryonic development.

We discovered that, similar to TKO foetuses, most QKO foetuses died before weaning and exhibited mostly similar anomalies to age-matched TKO controls. However, additional tissues manifested anomalies when all four pro-apoptotic proteins are removed. These included the kidneys and the female urogenital tract. These findings and the observation that full-length BID can promote some mitochondrial release of cytochrome *c* suggest that BID may perform additional functions in cell death during embryogenesis on top of its known BH3-only protein duties as an initiator of apoptosis.

Results

A large proportion of QKO mice die before weaning

We aimed to investigate whether BID played a role in developmental apoptosis, apart from its function as a BH3-only protein. The *Bid* gene is expressed broadly at low levels during embryogenesis (Diez-Roux *et al*, 2011; data accessed 28/04/2022 at http://www. informatics.jax.org/assay/MGI:4823474#euxassay_006342_01_id). $Bid^{-/-}$ mice are viable, fertile and overtly normal (Yin *et al*, 1999; Kaufmann *et al*, 2007). Therefore, a genetic background sensitised for the detection of such a role for BID was required. We previously defined the roles of apoptosis in mouse development using $Bok^{-/-}Bax^{-/-}Bak^{-/-}$ triple knockout (TKO) animals (Ke *et al*, 2018). These mice did not show the detectable levels of apoptosis (or necroptosis, pyroptosis and autophagy) and revealed the organs that relied on BAX-, BAK- and BOK-mediated apoptosis for morphogenesis. However, some organs in which apoptosis is evident during embryogenesis appeared surprisingly normal in $Bok^{-/-}Bax^{-/-}Bak^{-/-}$ TKO mice. Therefore, to determine if there was a role of BID as an effector of apoptosis alongside BAX, BAK and BOK, we generated $Bok^{-/-}Bax^{-/-}Bak^{-/-}Bid^{-/-}$ quadruple knockout (QKO) mice, using $Bok^{-/-}Bax^{-/-}Bak^{-/-}$ triple knockout (TKO) animals as controls.

Adult QKO mice (≥ 60 days of age) were obtained at a lower frequency than the expected Mendelian ratios. Only 2% of mice that survived to adulthood were QKO mice (10 of 498 animals in total, Fig 1A) and only 2.6% (15 of 576 total offspring) of animals that survived to weaning were QKO mice (≥ 21 days; Fig 1A). TKO foetuses were modestly significantly underrepresented at E18.5 (16.8% vs. 25%), whereas the frequency of QKO foetuses was not significantly different from the expected Mendelian frequency

A Observed and Expected Numbers of Offspring Genotypes from *Bok^-/-Bak^-/-Bax^+/-* and *Bok^-/-Bak^-/-Bax^+/-Bid^-/-* intercrosses.

Offspring of *Bok^-/-Bak^-/-Bax^+/-* x *Bok^-/-Bak^-/-Bax^+/-* matings					
Genotype	*Bok^-/-Bak^-/-Bax^+/+*	*Bok^-/-Bak^-/-Bax^+/-*	*Triple KO*	Total	*p* value
E18.5 - E19	65 (58)	128 (116)	39 (58)	232	0.02
Weaning	261(194)	495 (388)	20 (194)	776	< 0.0001
Adult	227 (173)	459 (346)	6 (173)	692	< 0.0001

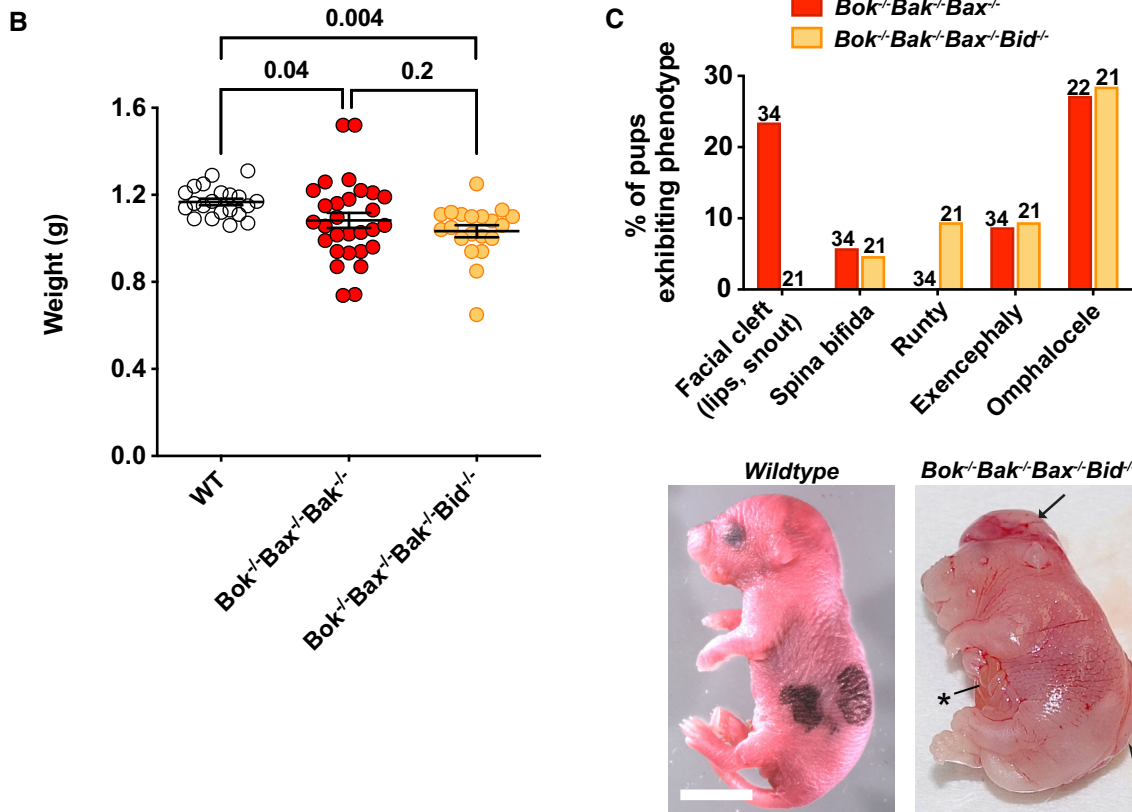| Offspring of *Bok^-/-Bak^-/-Bax^+/-Bid^-/-* x *Bok^-/-Bak^-/-Bax^+/-Bid^-/-* matings					
Genotype	*Bok^-/-Bak^-/-Bax^+/+Bid^-/-*	*Bok^-/-Bak^-/-Bax^+/-Bid^-/-*	*Quadruple KO*	Total	*p* value
E18.5 - E19	33 (29.25)	58 (58.5)	26 (29.25)	117	0.7
Weaning	213 (144)	348 (288)	15 (144)	576	< 0.0001
Adult	165 (124.5)	323 (249)	10 (124.5)	498	< 0.0001

B

C

Figure 1.

(22% vs. 25%). However, comparing the frequencies of TKO to QKO foetuses at E18.5 to each other revealed no significant difference (Pearson's Chi-square and Fisher's exact test, $P = 0.4$). Similarly, the frequencies of TKO and QKO mice were not significantly different at weaning ($P = 0.4$) or at reaching adulthood ($P = 0.2$). These findings suggest that like TKO mice, the majority of QKO offspring may harbour developmental anomalies that are incompatible with post-natal survival.

Therefore, E18.5 QKO foetuses were examined physically and microscopically. The weight of TKO foetuses was reduced on average by 7% compared to age-matched WT controls (Fig 1B). Pups with the additional loss of BID on top of the absence of BAX, BAK and BOK displayed an 11% reduction in weight compared to WT controls (Fig 1B). Some QKO pups were already dead upon harvest, and these animals usually exhibited major abnormalities (Fig 1C, bottom panel). A portion of QKO mutants displayed dorsal and

ventral midline fusion defects, such as exencephaly, spina bifida and omphalocele, and these phenotypes were also observed at similar frequencies in TKO animals (Ke *et al*, 2018). While 23.5% of TKO foetuses (34 examined in total) exhibited various types of externally visible facial clefts, this was not observed in the 21 QKO pups examined (Fig 1C).

All QKO foetuses displayed heart vessel and/or aortic arch anomalies

E18.5 QKO foetuses were examined under a dissection microscope to determine whether additional anomalies were present (Fig 2A). We discovered that QKO mice displayed similar defects to their TKO counterparts; however, some abnormalities were more frequently observed in one or the other genotype. Cleft palate occurred more frequently in TKO compared to QKO pups (Fig 2A and G vs. D). Curled tail tips (Fig 2A and E vs. B) and excess tissue protrusions on the anterior or posterior edges of the forelimbs were seen more frequently in the QKO compared to TKO foetuses (Fig 2A and F,I vs. C), whereas the frequency of skin protrusions on the hindlimbs was similar in the TKO and QKO foetuses (Fig 2A and E,H vs. B).

Strikingly, all QKO mutants exhibited a developmental defect in the great vessels of the heart (Fig 2A and J). These consisted of minor right subclavian artery (RSA) defects—for example, a very thin RSA resulting from faulty vessel remodelling, aberrant origin of the RSA, absence of the RSA (Fig 2L vs. K), as well as severe defects, such as a persistent truncus arteriosus and an abnormal pulmonary trunk and ductus arteriosus (Fig 2M vs. K). In the latter condition, the aorta failed to develop an aortic arch.

Oxygenated blood from the lungs is therefore not provided to the body and, instead, deoxygenated blood circulates. This is likely to lead to death after birth, at the time when blood oxygenation via the placenta is replaced by oxygenation via the lungs.

The additional loss of BID in QKO foetuses led to the retention of extra tissue in multiple regions of the head compared to TKO foetuses

E18.5 QKO foetuses ($n = 3$–4) were examined histologically for internal developmental abnormalities in comparison to both TKO ($n = 3$–4) and WT ($n = 2$) controls. Coronal (head) and transverse (body) serial sections from all animals were carefully examined and equivalent rostro-caudal levels were compared.

In general, we observed more tissue mass in various regions of the head of QKO foetuses compared to the TKO foetuses. In QKO mutant animals, the forebrain subventricular zone, a region of the brain populated by neural stem and progenitor stem cells, was significantly expanded (Figs 3A and D, and EV1A). More bone and cartilage tissues were observed in the nasal capsule (Figs 3B and D, and EV1A). QKO mutants had a prominently larger tongue (Figs 3C and D, and EV1A) compared to the TKO controls. The olfactory bulbs of QKO mutant animals showed a tendency to be larger compared to those from both TKO controls (Fig EV1B).

The embryonic hyaloid vessels in the eye nourish the developing vitreous body, lens and retina, forming vascular network on the posterior surface of the lens and throughout the hyaloid cavity (Ito & Yoshioka, 1999). These vessels then regress to allow for an
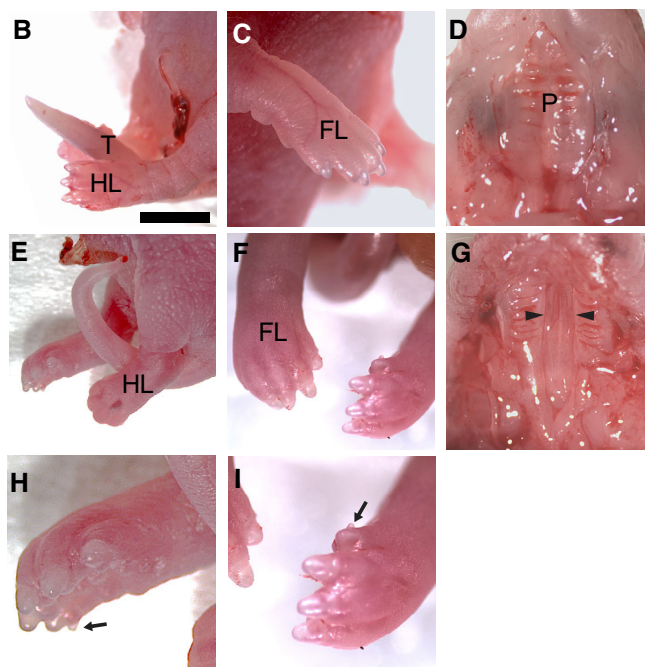
A Macroscopic anomalies
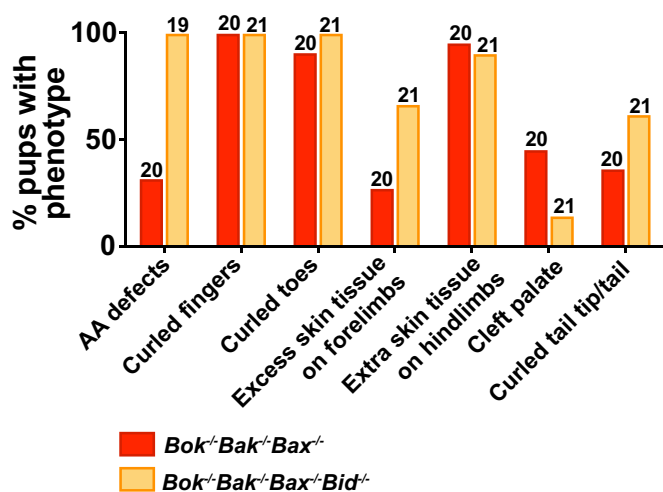
J Aortic arch and vessel anomalies
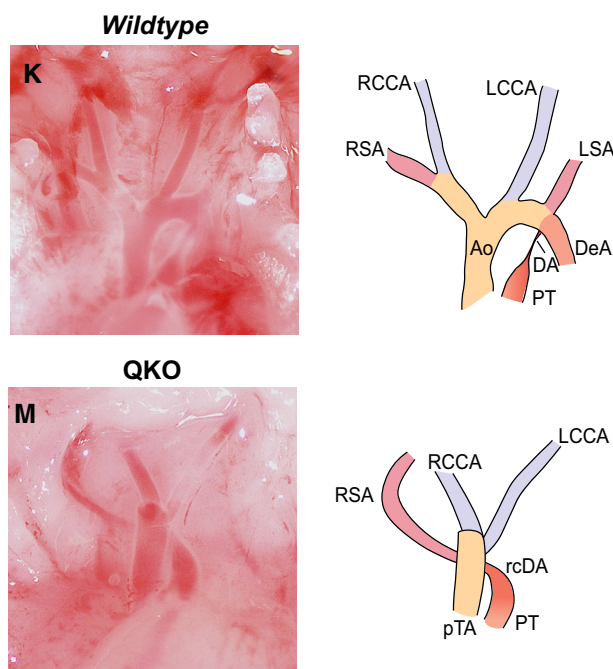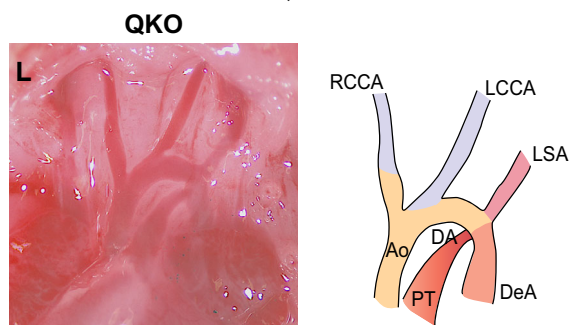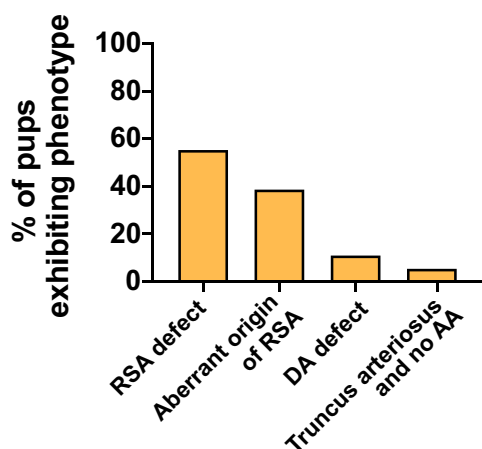
Figure 2.

unobstructed light path and development of optimal visual function. Apoptotic cells have been observed during hyaloid vessel regression (Taniguchi *et al*, 1999). Histological examination revealed that QKO foetuses displayed an increase in hyaloid vasculature compared to TKO controls (Fig 4A–D).

QKO animals exhibited defects in kidney development

Transverse serial sections of the bodies of E18.5 QKO (*n* = 4), TKO (*n* = 4) and WT (*n* = 2) foetuses were examined. The kidneys of WT (Fig 5A and D) and TKO pups (Fig 5B and E) were not
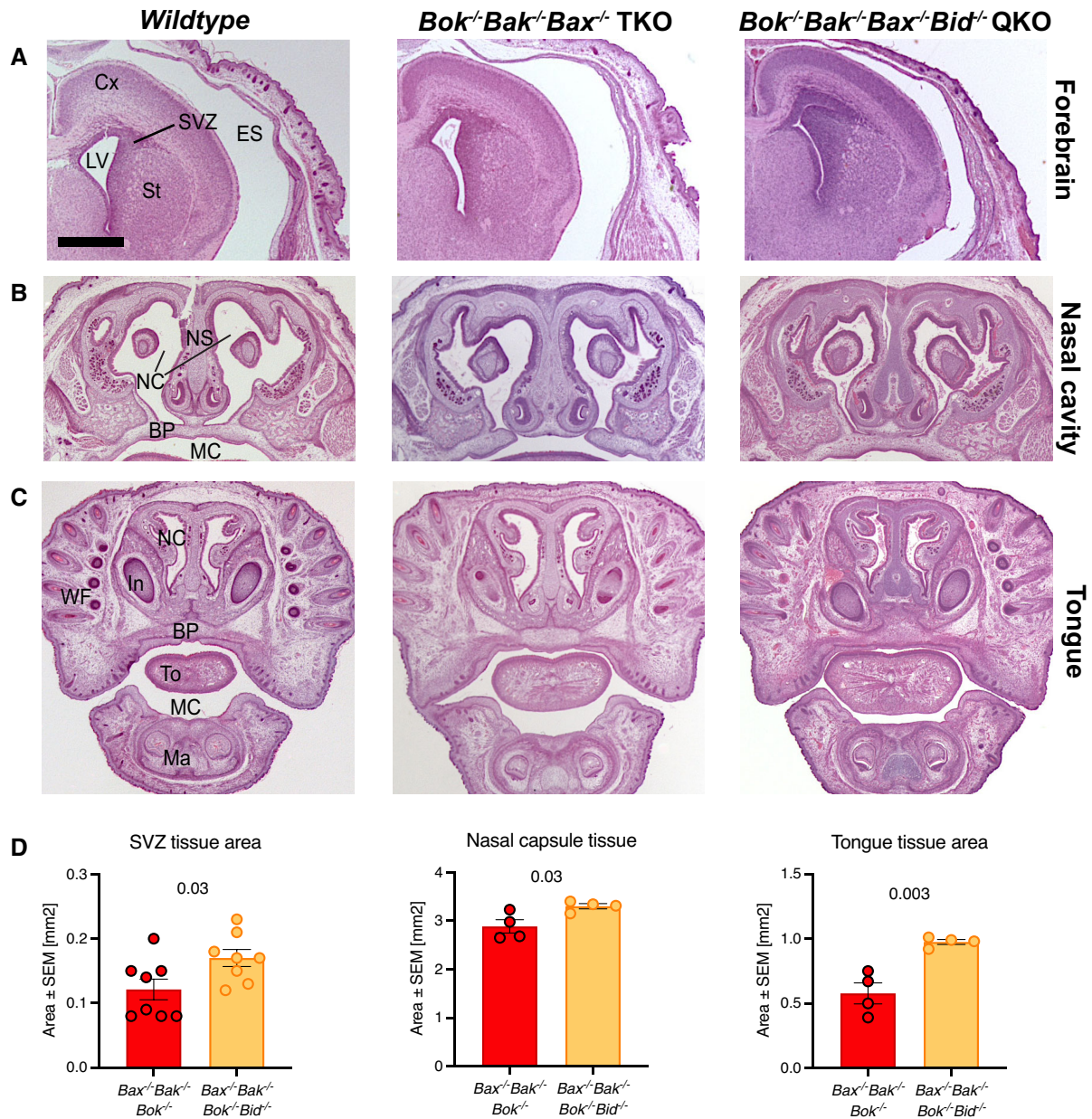
Figure 3. *Bok$^{-/-}$Bak$^{-/-}$Bax$^{-/-}$Bid$^{-/-}$* quadruple knockout (QKO) foetuses displayed brain and craniofacial anomalies at E18.5.

A–C Heads of E18.5 foetuses were serially sectioned in coronal orientation and stained with H&E. Representative images of rostro-occipital level-matched sections from age-matched wild-type (n = 2), *Bok$^{-/-}$Bak$^{-/-}$Bax$^{-/-}$* triple knockout (TKO; n = 4) and QKO foetuses (n = 4) depicting the forebrain, nasal cavity and tongue are shown. BP, bony palate; Cx, cerebral cortex; ES, epidural space; In, incisor; LV; lateral ventricle; Ma, mandible; MC, mouth cavity; NC, nasal cavity; NS, nasal septum; St, striatum; SVZ, subventricular zone; To, tongue; WP, whisker follicles. The length of the scale bar displayed in A equals 850 μm in A, 1,200 μm in B, C.

D Morphometric assessment of indicated tissue areas. Data of individual animals are displayed as circles with means and standard error of the mean. Data were analysed by unpaired, two-tailed Student's t-test. Related data normalised to mean bodyweight are displayed in Fig EV1.

Source data are available online for this figure.

appreciably different. In contrast, kidneys from QKO mice showed clear evidence of glomerular cysts characterised by an enlarged Bowman's space with a compressed glomerulus (Fig 5C and F). In two of the four QKO foetuses examined, the renal papilla was either absent or severely reduced in size (Fig 5C, indicated by asterisk*). Instead of a normal rounded cone projecting into the renal pelvis,

the medulla contained expanded regions of stroma and potentially shortened or bent papillae (Fig 5A vs. C).

Hydronephrosis is a condition where the renal pelvis and calyces are dilated as the result of an obstruction in the urinary tract, affecting the normal drainage of urine. This can be caused by a downstream obstruction but is also associated with intrinsic
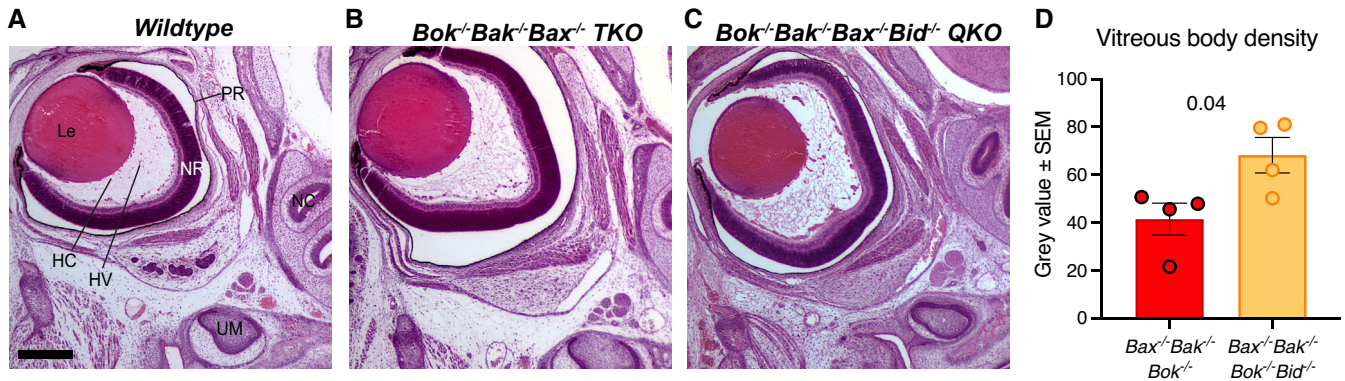
Figure 4. Anomalies in the eyes of $Bok^{-/-}Bak^{-/-}Bax^{-/-}Bid^{-/-}$ quadruple knockout (QKO) foetuses at E18.5 of development.

A–C Representative H&E-stained coronal serial sections of the eye from E18.5 wild-type (*n* = 2), $Bok^{-/-}Bak^{-/-}Bax^{-/-}$ triple knockout (*n* = 3) and $Bok^{-/-}Bak^{-/-}Bax^{-/-}Bid^{-/-}$ quadruple knockout (*n* = 3) foetuses.

D Densitometry of hyaloid cavity tissue section as an assessment of blood vessel endothelial cells present. Data of individual animals are displayed as circles with means and standard error of the mean and were analysed by unpaired, two-tailed Student's *t*-test.

Data information: HC, hyaloid cavity (future vitreous body); HV, hyaloid vessels; Le, lens; NC nasal cavity; NR, neural retinal; PR, pigmented retina; UM, upper molar. The length of the scale bar displayed in A equals 1,470 μm in all figure panels.

Source data are available online for this figure.
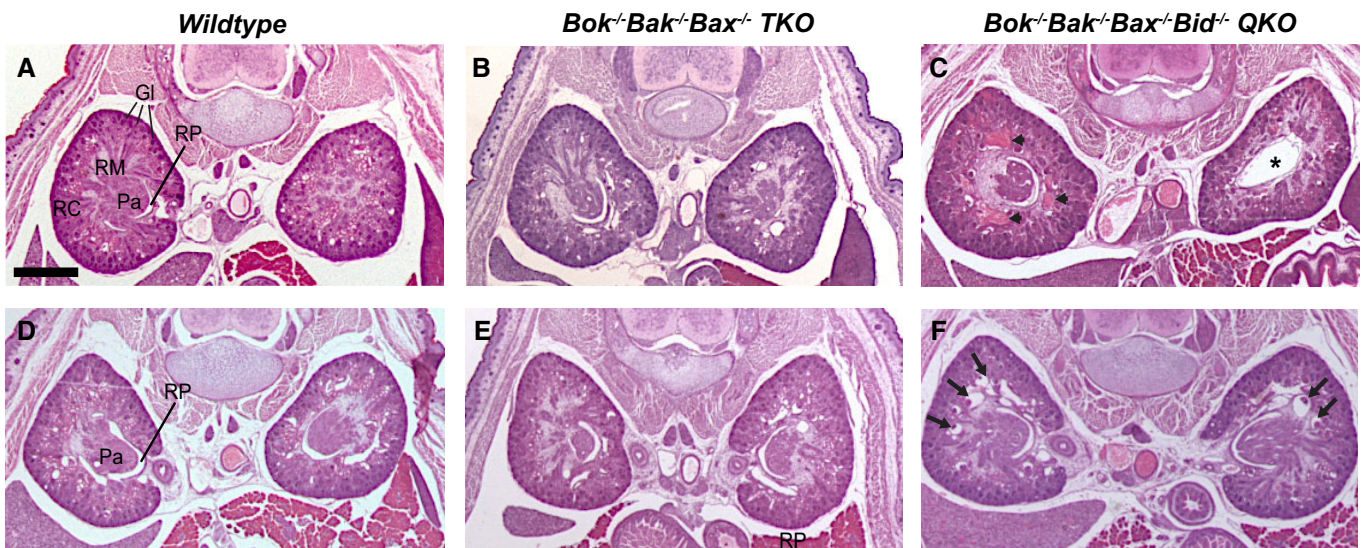
Figure 5. $Bok^{-/-}Bak^{-/-}Bax^{-/-}Bid^{-/-}$ quadruple knockout (QKO) foetuses displayed abnormal kidney morphology.

A–F Representative, rostro-caudal-level-matched sections selected from H&E-stained serial sections at the level of the kidneys from E18.5 wild-type (*n* = 2), $Bok^{-/-}Bak^{-/-}Bax^{-/-}$ triple knockout (TKO; *n* = 4) and QKO foetuses (*n* = 4). Wild-type foetus (A, D). $Bok^{-/-}Bak^{-/-}Bax^{-/-}$ triple knockout foetuses (B, E). $Bok^{-/-}Bak^{-/-}Bax^{-/-}Bid^{-/-}$ quadruple knockout foetuses (C, F).

Asterisks (*) in Fig C indicate the absence of a normal renal papilla, arrowheads indicate blood filled spaces. Arrows in panel F denote the presence of glomerular cysts. Gl, glomeruli; Pa, papilla; RC, renal cortex; RM, renal medulla; RP, renal pelvis. The length of the scale bar displayed in A equals 1,270 μm in A–D, 1,590 μm in E, 1,430 μm in F.

developmental defects within the metanephros itself. It most commonly affects one kidney but can also involve both kidneys. Among the offspring of $Bok^{-/-}Bax^{+/-}Bak^{-/-}$ intercross matings, we observed a rare case of hydronephrosis (1 in 681). In contrast, when BID was lost in addition, we observed 11 hydronephroses in both kidneys among 464 offspring of $Bok^{-/-}Bax^{+/-}Bak^{-/-}Bid^{-/-}$ intercross matings, a 16-fold higher incidence (Fisher's exact test, *P* = 0.0003; Fig EV2). This suggests that the loss of BID specifically may compromise urinary tract development when BOK and BAK are absent. The observed glomerular cysts in QKO pups (Fig 5F) indicate a level of congestion in urine drainage downstream that could give rise to hydronephrosis, as

observed at higher frequency in animals lacking BID, BOK and BAK (Fig EV2).

QKO female foetuses exhibited abnormalities in urogenital tract development

In E18.5 WT female pups (Fig 6), bilateral paramesonephric ducts (also known as Mullerian ducts) form the future uterine horns. They descend towards the midline and pass in front of the ureters, meeting behind the neck of the bladder (Fig 6A and B). Only the caudal portions of lumina of the ducts fuse to form a common cervical canal (i.e. the future cervix; Fig 6C and D). The left and right ureters extend from the collecting system of the kidneys and enter the bladder, where urine is stored until it is excreted from the body via the urethra. In female mouse foetuses, the vaginal–vulval opening is blocked by the sino-vaginal bulb at E18.5 (Georgas et al, 2015) and does not open to the skin until after birth (Fig 6E and F).

In age-matched TKO female pups (n = 2; Fig 7), we discovered that although the paramesonephric ducts are directed towards the midline and become apposed, their lumina remained separated by intervening walls (Fig 7A). The ducts then moved further apart, with the left duct ending blind first (Fig 7B and C), followed by the right duct (Fig 7D–F). In both female TKO animals examined, a region of the urethra that may correspond to the level of the prostate gland in males, contained unusually enlarged tissue for a female (Fig 7E, indicated by white arrowhead). We also noted the presence of aberrant tube-like tissue on the outer side of both paramesonephric ducts (blue arrows in Fig 7D–H). These excess tubes could reflect remnants of the sexually indifferent state that should have regressed in females at this stage of development (e.g. mesonephric/Wolffian ducts, which would develop in males to form the epididymis and vas deferens).

Like TKO foetuses, all QKO foetuses (n = 3; Figs EV3, EV4, and 8) examined also displayed defects in paramesonephric duct fusion, an excess tissue mass in the urethra (indicated by white arrowhead), extra tubules, as well as additional structural anomalies in urogenital tract development. There were some differences between the individual QKO mutants examined, but their defects were generally more severe compared to those seen in the TKO animals.

One of the female QKO foetuses had bilateral paramesonephric ducts that remained further apart than in all TKO and the other two QKO animals examined (Fig EV3A and B). The failure of the bilateral ducts to fuse into a single canal resulted in the formation of an unusual cervical structure; the two tissue structures surrounding the paramesonephric ducts remained distinct (Fig EV3C). The right duct

was not fully canalised throughout its length, from the observation of epithelial tissue in the middle of the lumen (Fig EV3B). Similar to TKO animals, the left paramesonephric duct terminated prior to the right (Fig EV3C vs. D), and parallel to the right paramesonephric duct was an additional tube that was connected to the urethra (blue arrows in Fig EV3E–K). In addition, this specimen displayed a profound distension of the left ureter, which abnormally fused over an extended area not only with the bladder but also ectopically with the urethra (Fig EV3A–C).

The second female QKO foetus similarly displayed abnormal paramesonephric ducts (Fig EV4A) and abnormal duct-like structures with a distinct epithelium, which were peripheral to the paramesonephric ducts (blue arrows in Fig EV4B–K) and connected to the urethra. This animal harboured an additional tube, which emanated from the left kidney parallel to the left ureter. Where the ureter fused with the bladder, this additional tube continued parallel to the paramesonephric duct, then fused to the urethra (pointed out with green arrow in Fig EV4A–H). The course of the additional tube suggested it was a ureter duplication. Ureter duplications occur as common upper urinary tract malformations in humans (Smith & Dunn, 1979).

The last female QKO foetus we examined exhibited the most severe urogenital tract malformation. The left paramesonephric duct failed to form a consistent single channel (Fig 8A) and ended very prematurely (Fig 8B vs. C). We also noted the presence of superfluous oddly shaped tubes (blue arrows in Fig 8C–F). The openings of the intestinal, genital and urinary tracts were fused to form a single common cavity (Fig 8F and G), resulting in a persistent cloaca (Fig 8H and I).

Overall our data show that the anomalies observed in the urogenital tract were more severe in the QKO mice than in TKO mice.

High levels of BID can trigger partial cytochrome c release from isolated BAX/BAK/BOK-deficient mitochondria

To explore the mechanism by which BID might contribute to the additional anomalies observed in QKO mice compared to TKO mice, we investigated if different forms of recombinant human BID can release cytochrome c from mitochondria in mouse fibroblasts lacking the pore-forming BCL2 proteins, BAX, BAK and BOK. To measure even minor release of cytochrome c, flow cytometry was performed on fixed cells co-stained with antibodies against cytochrome c and TOM20, the latter a protein in the mitochondrial outer membrane. In addition, BID proteins were added at levels estimated

Figure 6. H&E-stained serial sections of the urogenital region in a female wild-type foetus at E18.5 of development. ▶

Schematic drawings (from left to right) depict orientation of the sections and ventral and oblique lateral aspects of the kidneys, ureters, bladder (*), ovary, right (R) and left (L) paramesonephric ducts, urethra (Ur) and rectum (#).

A, B The left (L) and right (R) paramesonephric ducts are directed caudally and towards the midline (compare panel A–B). Black arrows indicate the ureters that descend (and open into the lumen of the bladder indicated by asterisk *). Black arrowhead in panel B denotes the site of apposition of both paramesonephric ducts. #, Rectum.

C Paramesonephric ducts fuse in the midline, posterior to the bladder. Dashed oval outlines the future cervix (caudal region of the fused L and R ducts). Ur, urethra.

D, E Paramesonephric ducts have fused to form a single lumen that gradually terminates as the sections proceed caudally. Dashed oval outlines the future cervix (caudal region of the fused L and R ducts). Ur, urethra.

F The reproductive tract lumen ends blind (indicated by red arrowhead). Opening of the vaginal cavity to the skin occurs later in development.

Data information: Representative images of selected levels of serial section are shown. The length of the scale bar displayed in A equals 580 μm in A–C, 540 μm in D–F.
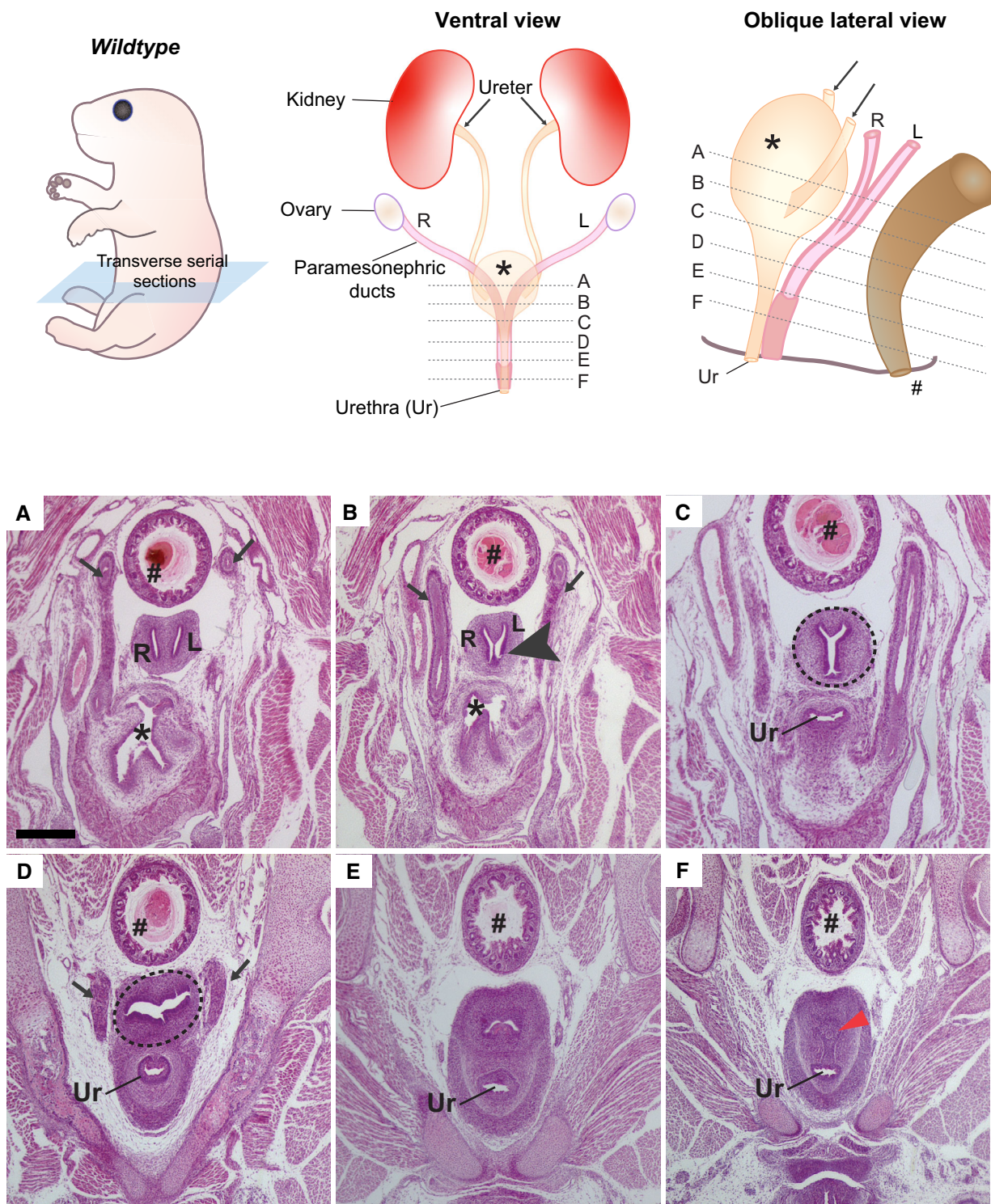
Figure 6.

to be > 10-fold higher than that in cultured human leukaemia cells (Fig 9A). We compared the full-length protein (FL-BID) with caspase-8-cleaved BID (cBID) that retains both the p15 (tBID) and p7 fragments (Li *et al*, 1998; Luo *et al*, 1998; Chou *et al*, 1999; Zha *et al*, 2000).

As positive controls, permeabilised DKO MEFs manipulated to express human BAK were incubated with 30 nM of the BIM BH3 peptide, cBID or FL-BID. As expected, staining for cytochrome *c* was greatly decreased in all cells (Fig 9B), indicating that BIM BH3 peptide and cBID had activated BAK to trigger cytochrome *c* release from all
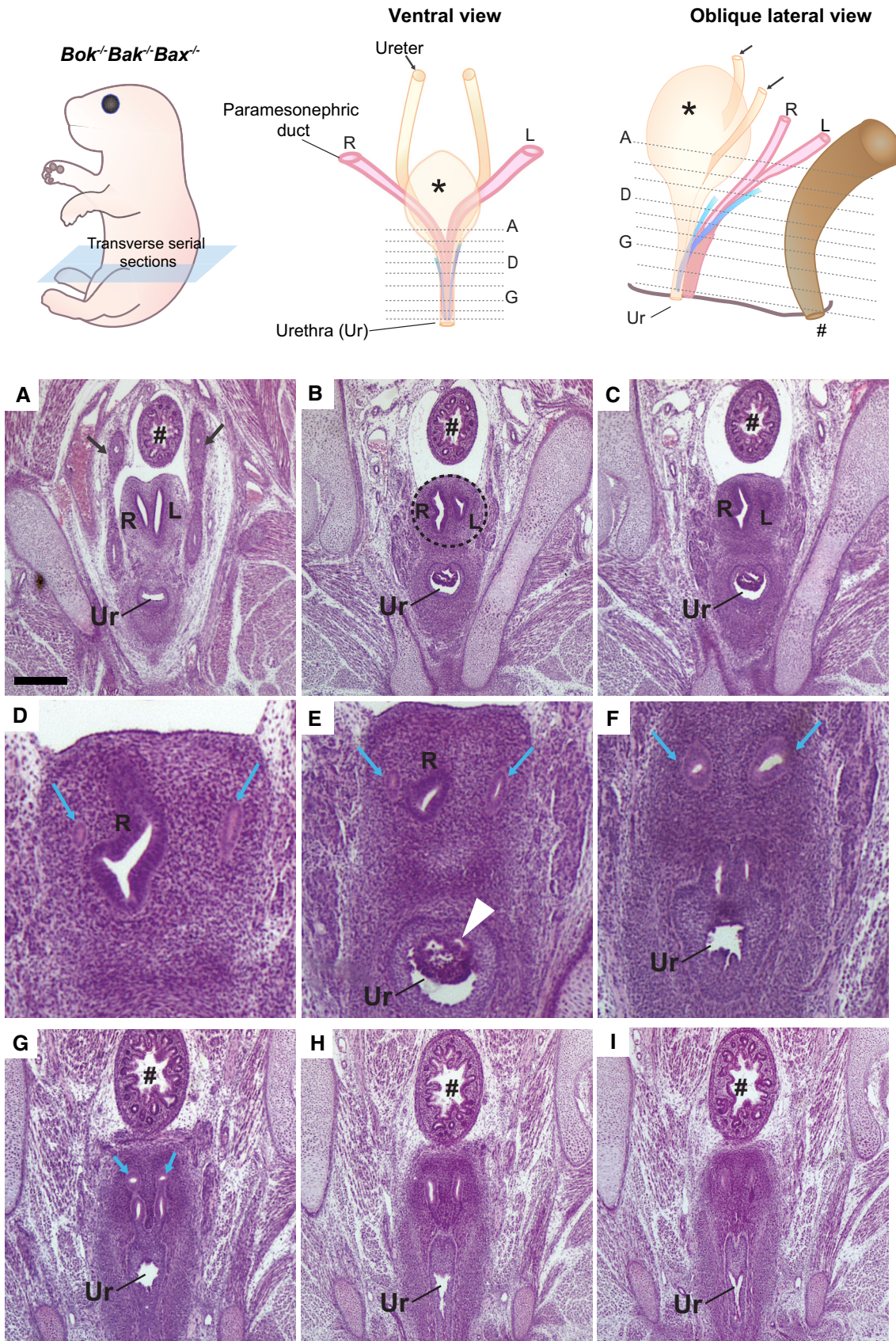
Figure 7.

Figure 7.   H&E-stained serial sections of the urogenital region in a female *Bok*$^{-/-}$*Bak*$^{-/-}$*Bax*−/− TKO foetus at E18.5 of development.

Schematic drawings (from left to right) depict orientation of the sections and ventral and oblique lateral aspects of the ureters, bladder (*), right (R) and left (L) paramesonephric ducts, urethra (Ur), rectum (#) and excess ducts (blue).

A   The left (L) and right (R) paramesonephric ducts are directed towards the midline but do not fuse. Arrows indicate the ureters. Ur, urethra; #, rectum.
B, C   The left (L) paramesonephric duct decreases in diameter and ends before the right (R) paramesonephric duct. Dashed oval outlines where the future cervix should be caudal region of the L and R ducts.
D–F   The lumen of the right (R) paramesonephric duct gradually diminishes and ends as the serial sections progress caudally and have terminated by panel F. Blue arrows indicate excess ducts (possibly remnant Wolffian ducts). White arrowhead indicates the presence of excess tissue in the urethra (Ur).
G–I   Fusion of excess ducts with the urethra. Blue arrows indicate excess ducts (possibly remnant Wolffian ducts).

Data information: Representative images of selected levels of serial section are shown. The length of the scale bar displayed in A equals 1,300 μm in A, B, G–I, 1,200 μm in C, 730 μm in D, 650 μm in E, 640 μm in F.

mitochondria within all cells. FL-BID was also effective at activating BAK, perhaps due to partial unfolding of the protein to expose its BH3 domain. TOM20 levels remained unchanged, consistent with BAK (and BAX) porating the outer membrane without causing loss of the membrane or the proteins embedded within it (Fig 9C).

When TKO MEFs were treated in the same way, little change in cytochrome *c* staining was observed, even if BIM BH3 peptide or BID were added at 300 nM (Fig 9B). However, if FL-BID was supplemented with the BIM BH3 peptide or with cBID, a small decrease in cytochrome *c* content of most cells was evident, with no decrease in TOM20 staining (Fig 9B and C). These findings suggest that a subpopulation of mitochondria within each cell were porated by the combination of FL-BID with an 'activator', such as the BIM BH3 peptide or cBID.

Discussion

We have previously shown that the absence of all identified effectors of apoptosis, BAX, BAK and BOK, abrogated detectable developmental apoptosis (Ke *et al*, 2018). We defined the developmental processes that require apoptosis as brain and retina cell homeostasis, blood cell homeostasis, removal of interdigital tissue and fusion of the midline body wall, palate and lower parts of the bilateral Müllerian ducts at the level of the corpus uteri (Ke *et al*, 2018). However, the development of other organs, such as the metanephros (Koseki *et al*, 1992), cloaca (Sasaki *et al*, 2004) and the insertion of the ureters into the bladder (Batourina *et al*, 2005), had previously been proposed to require apoptosis. This left open the possibility that although the absence of BAX, BAK and BOK abrogated detectable developmental apoptosis, other BCL-2 family

members might contribute to developmental apoptosis in a relatively subtle but essential manner.

In this study, we have investigated whether the pro-apoptotic BCL-2 family protein BID plays a role, independent from its function as a BH3-only protein, in developmental apoptosis. We assessed the role of BID on a sensitised *Bok*$^{-/-}$*Bax*$^{-/-}$*Bak*$^{-/-}$ background comparing *Bok*$^{-/-}$*Bax*$^{-/-}$*Bak*$^{-/-}$*Bid*$^{-/-}$ QKO to *Bok*$^{-/-}$*Bax*$^{-/-}$*Bak*$^{-/-}$ TKO animals, because mice lacking BID are viable and fertile and do not show overt anomalies (Yin *et al*, 1999; Kaufmann *et al*, 2007). Our results reveal that BID is likely to contribute to developmental apoptosis in a way not previously appreciated. Similar to TKO mice, QKO mice showed defects in brain and retina cell homeostasis, removal of interdigital tissue and fusion of the midline body wall, and lower parts of the bilateral Müllerian ducts. The frequency of occurrence of these anomalies varied to some extent between QKO and TKO mice, but no strong trend was discernible. However, while an excess in the size of the brain region containing neural stem and progenitor cells was already observed in *Bax*$^{-/-}$*Bak*$^{-/-}$ DKO (Lindsten *et al*, 2000) and TKO mice (Ke *et al*, 2018), this neurogenic region containing neural stem cells and rapidly dividing neuronal progenitor cells was substantially greater in QKO mice. Importantly, QKO mice showed a completely novel phenotype: major anomalies of the urogenital tract, including abnormal Mullerian duct fusion, kidney anomalies including glomerular cysts and anomalous papillary formation, partially penetrant double ureter, mis-insertion of the common nephric duct into the neck of the bladder and hydronephrosis. These findings suggest a role of BID in developmental apoptosis in the urinary tract and the female genital tract. These major organ systems affected in QKO mice in addition to those affected in TKO have not been examined in detail in *Bid*$^{-/-}$ single KO mice. However, intercrosses of *Bid*$^{+/-}$

Figure 8.   H&E-stained serial sections of the urogenital region in a female *Bok*$^{-/-}$*Bak*$^{-/-}$*Bax*$^{-/-}$*Bid*−/− QKO foetus at E18.5 of development.

Schematic drawings (from left to right) depict orientation of the sections and ventral and oblique lateral aspects of the ureters, bladder (*), right (R) and left (L) paramesonephric ducts, urethra (Ur), rectum (#) and excess ducts (blue).

A   Black arrows indicate ureters. The bladder is indicated by an asterisk *. #, Rectum; L, left paramesonephric duct; R, right paramesonephric duct.
B, C   The left (L) paramesonephric duct ends before the right (R) paramesonephric duct. Blue arrows from panel C onwards indicate excess ducts. B, Dashed oval black outlines where the future cervix should develop (caudal region of the L and R ducts).
D–G   The lumina of the right (R) paramesonephric duct and the rectum gradually approach the urethra and fuses with the urethra. Blue arrows indicate excess ducts (possibly remnant Wolffian ducts). White arrowhead indicates the presence of excess tissue in the urethra (Ur). The rectum (#) fuses with the urethra (Ur). Dashed yellow outline indicates the fused tissue mass of rectum, paramesonephric duct and urethra (F, G).
H, I   After fusion of the right paramesonephric duct, rectum and urethra, a common orifice, known as a persistent cloaca (cloacal deformity), remains. Dashed yellow outline indicates the fused tissue mass of rectum, paramesonephric duct and urethra.

Data information: Images of selected levels of serial sections are shown. Further *Bok*$^{-/-}$*Bak*$^{-/-}$*Bax*$^{-/-}$*Bid*$^{-/-}$ QKO female foetuses are depicted in Figs EV3 and EV4. The length of the scale bar displayed in A equals 1,230 μm in A, 1,320 μm in B, 1,070 μm in C, G–I, 1,000 μm in D, 800 μm in E, 760 μm in F.
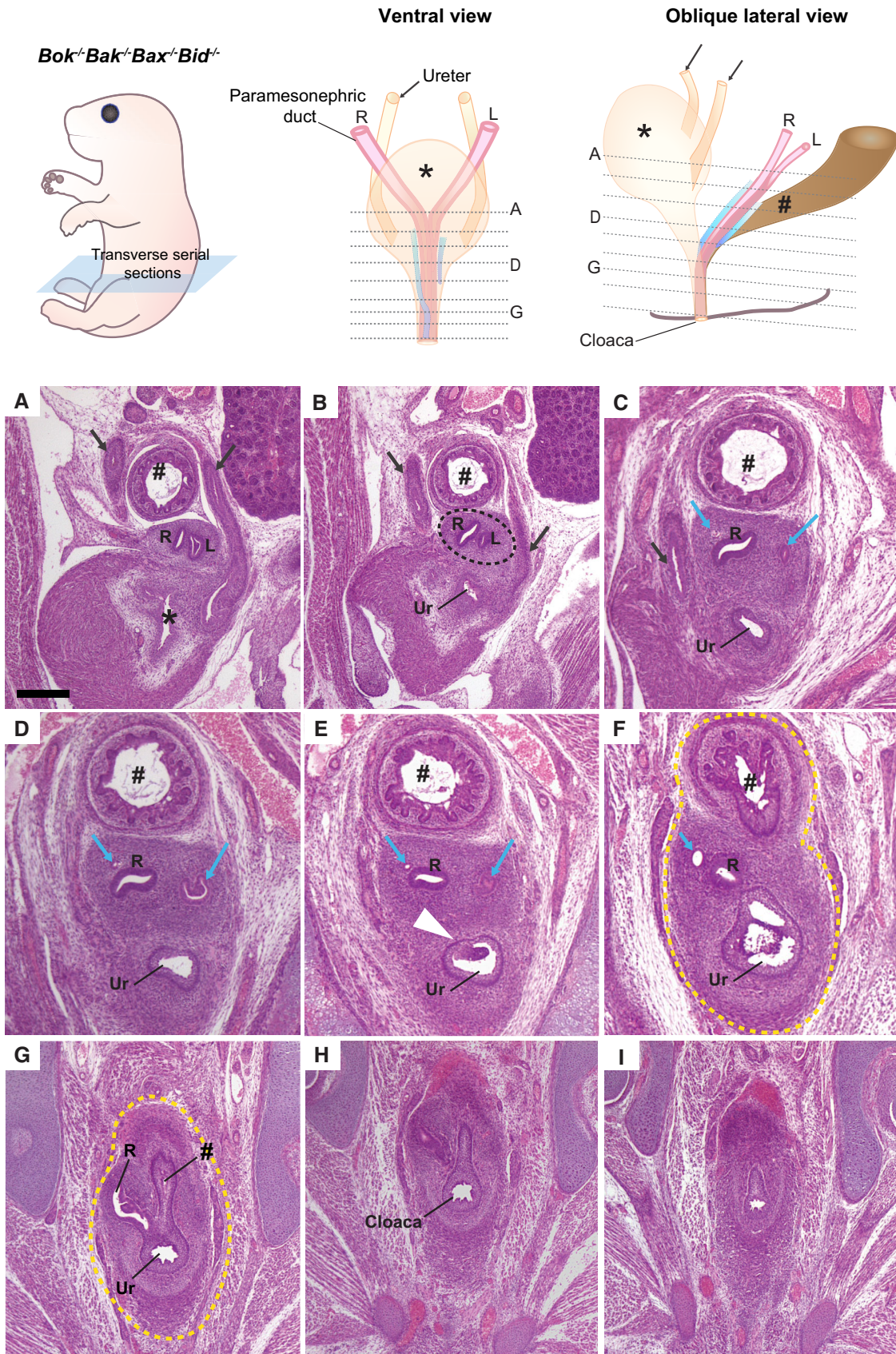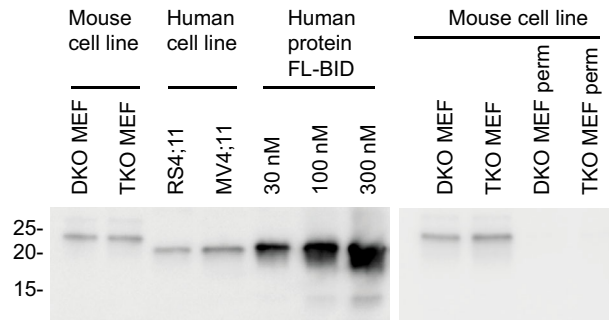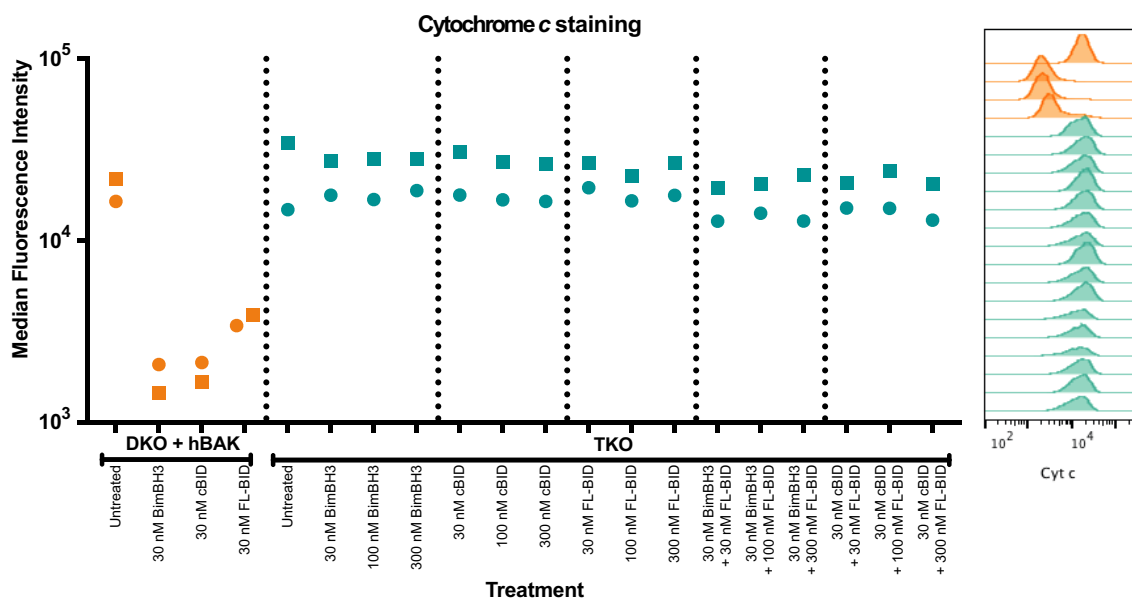
Figure 8.
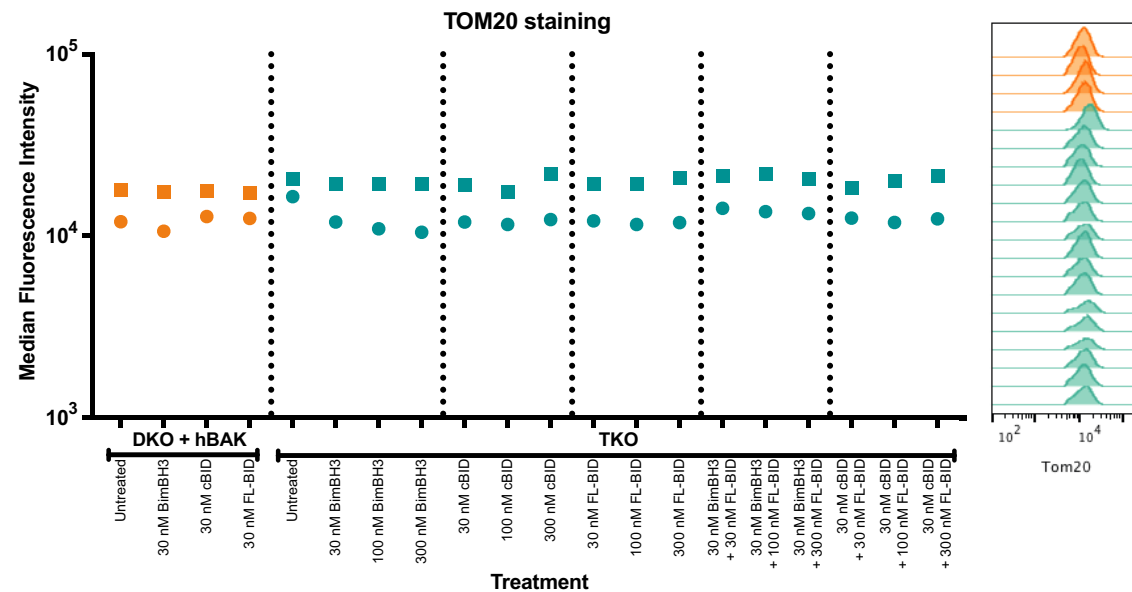
A

WB: rat anti-hBID (2D1)

B

C

Figure 9.

Figure 9. BID can trigger partial cytochrome *c* release from isolated BAX/BAK/BOK-deficient mitochondria when applied at high levels.

A   Estimation of BID protein levels in TKO MEFs. DKO MEFs manipulated to express human BAK, TKO MEFs and two human leukaemia cell lines RS4;11 and MV4;11 were lysed and analysed by Western blot for BID levels, using a rat monoclonal antibody raised against human BID (anti-hBID clone 2D1) that also recognises mouse BID. Also present are samples of the human full-length (FL)-BID protein added at the equivalent concentrations used in (B) and (C). On the right gel, duplicate samples of DKO and TKO cells and permeabilised DKO and TKO cells (from B and C) showing that endogenous mouse BID is cytosolic in these cells. Data shown are representative of two independent experiments.

B, C   Partial cytochrome *c* release by FL-BID from mitochondria of TKO MEFs when combined with BIM BH3 peptide or cBID. DKO MEFs manipulated to express human BAK or TKO MEFs were permeabilised, and then, the cells incubated with the indicated concentrations of Bim BH3 peptide, cBID or FL-BID, alone or in the indicated combinations, at 30°C for 30 min. Cells were then co-stained for cytochrome *c* and TOM20 and analysed by flow cytometry. The left hand panels show median fluorescence data from replicate experiments (squares denote experiment 1, circles denote experiment 2). Right hand panels show histograms of cytochrome *c* staining and TOM20 staining from experiment 2 (treatments are as listed in the left-hand panels).

Source data are available online for this figure.

heterozygous mice yielded the expected portion of $Bid^{-/-}$ offspring, $Bid^{-/-}$ mice live a normal lifespan and $Bid^{-/-}$ males and females are fertile (Kaufmann *et al*, 2007) and so it is highly likely that any anomalies that might occur in the $Bid^{-/-}$ single KO upper urinary tract or female genital tract would at most be minor. These considerations suggest that this role of BID is redundant with BAX, BAK and BOK and only revealed in their absence.

Of note, the observed additional anomalies in QKO mice are in an organ system requiring tissue remodelling processes previously proposed to involve apoptosis (Glucksmann, 1951). The most prominent kidney anomaly were glomerular cysts. While less common than genetic cystic disease, such as polycystic kidney disease or nephronophthisis, glomerular cysts have been described in some forms of genetic renal dysplasia, including in association with *HNF1B* (Bingham *et al*, 2001) and *UMOD* mutations (Bolar *et al*, 2016). However, they can also indicate the presence of hydronephrosis. Hence, it is not clear if this abnormality is arising due to an inherent defect in apoptosis within the kidney or from anomalies downstream around ureter insertion.

The formation of the permanent kidney, the metanephros, requires reciprocal induction events between the Wolffian duct/mesonephric duct and the metanephric mesenchyme (Dressler, 2009; Little & McMahon, 2012). In response to the secretion of glial-derived neurotrophic factor (GDNF) from the metanephric mesenchyme, the nephric duct expressing the GDNF receptor RET swells to form a ureteric bud, which extends to the mesenchyme before commencing dichotomous branching and giving rise to both the ureter and the collecting ducts of the kidney. The position and number of ureteric buds are controlled via BMP, WNT5A and ROBO expression from the mesoderm adjacent to the nephric duct, with an imbalance in signalling or mutations in a number of genes causing ureter bud duplication, for example., *Spry1* (Basson *et al*, 2005, 2006); *Robo2* (Wainwright *et al*, 2015). Ureter duplications are the most common upper urinary tract malformation in newborn humans (Smith & Dunn, 1979). Apoptosis in kidney development has previously been reported (Koseki *et al*, 1992); however, its requirement in this tissue has not been clearly revealed by the combined deletion of *Bax* and *Bak* (Lindsten *et al*, 2000) or even *Bax*, *Bak* and *Bok* (Ke *et al*, 2018). Conversely, excessive apoptosis in the developing kidney has been observed as a result of the absence of pro-survival BCL-2 (Veis *et al*, 1993; Nakayama *et al*, 1994; Kamada *et al*, 1995; Sorenson *et al*, 1995), which can be rescued by concomitant loss of one or two alleles of the *Bim* gene (Bouillet *et al*, 2001). Similarly, loss of specific transcription factors,

transcriptional co-activators or growth factors required for metanephros development can cause excessive apoptosis in the developing kidney (e.g. WT-1 (Kreidberg *et al*, 1993); GDNF (Sánchez *et al*, 1996); Eya1 (Xu *et al*, 1999); Sall1 (Nishinakamura *et al*, 2001)). However, there appears to be no report of the consequence of too little apoptosis in kidney development.

The defects observed in QKO mice suggested the presence of glomerular cysts and at least one example of an apparently aberrant or shortened papilla. Kim *et al* (1996) have shown in the rat that the final elongation of the loops of Henle to form the thin ascending limbs occurs postnatally and is associated with apoptosis at remodelling of the existing thick ascending limb. Hence, it is possible that both the cystic glomeruli and the short papilla arise due to a lack of apoptosis in final kidney maturation. The presence of hydronephrosis at a higher rate in mice lacking BOK, BAK and BID than in genotypes containing BID appears to be related to anomalies in the insertion into the bladder neck, a process also known to require apoptosis (Batourina *et al*, 2005). The observations that combined loss of *Bax*, *Bak*, *Bok* and *Bid* caused malformation of the kidney, and that deletion of the *Bid* gene could in some mice (also lacking *Bak* and *Bok*) cause hydronephrosis even in the presence of one or two functional alleles of *Bax* suggest that BID is particularly involved in executing apoptosis in the developing kidney.

Overall, based on the tissue localisation of the additional anomalies, particular roles for BID emerge in developmental apoptosis in the kidney/urinary tract, lower female reproductive tract and neural stem and progenitor cells. However, these roles appear to be redundant with BAK and BOK, as *Bid* knockout alone is not sufficient to cause these dysfunctions. In this context, BID does not act as a protein upstream of and activating BAX and BAK as a BH3-only protein, but as an effector parallel to BAX and BAK; otherwise, the absence of BAX and BAK would not have revealed these functions of BID. Our biochemical studies revealed that relatively high levels of full-length BID can promote a small release of mitochondrial cytochrome *c* when combined with a BIM BH3 peptide or cBID. This supports the notion that certain cells in TKO mice may still be able to benefit from this effect of BID to undergo developmentally programmed apoptosis. Whether, like BAX and BAK, FL-BID converts to an unfolded conformer to generate dimers and oligomers requires further investigation. A recent study provided evidence that the p15 fragment of BID (tBID) can also promote mitochondrial release of cytochrome *c* in a manner similar to BAX, BAK and BOK (Flores-Romero *et al*, 2022). Collectively, this work, older studies and our findings indicate that BID may promote MOMP through

three processes: (i) as a canonical BH3-only protein that after cleavage by caspase-8 inhibits pro-survival BCL-2 proteins and/or directly activates BAX and BAK directly, (ii) by permeabilising the mitochondrial outer membrane as the caspase-8 processed p15 form or (iii) as a full-length protein that structurally resembles BAX, BAK and BOK.

Finally, as observed for TKO mice (Ke *et al*, 2018), the rare survival of QKO mice suggests once again that developmental apoptosis may play a more restricted role than previously thought.

Materials and Methods

Mice

All animal experiments were performed with the approval of The Walter and Eliza Hall Institute Animal Ethics Committee and according to the Australian code of practice for the care and use of animals for scientific purposes (approval numbers: 2021.046, 2022.014). The generation of $Bok^{-/-}Bax^{-/-}Bak^{-/-}$ triple knockout (TKO) mice on a C57BL/6 background has been described previously (Ke *et al*, 2018). $Bok^{-/-}Bax^{-/-}Bak^{-/-}Bid^{-/-}$ quadruple knockout (QKO) animals were derived by crossing $Bok^{-/-}Bax^{+/-}Bak^{-/-}$ mice with $Bid^{-/-}$ mice (also generated on a C57BL/6 background) (Kaufmann *et al*, 2007). Following subsequent rounds of breeding, $Bok^{-/-}Bax^{+/-}Bak^{-/-}Bid^{-/-}$ animals were intercrossed to generate $Bok^{-/-}Bax^{-/-}Bak^{-/-}Bid^{-/-}$ QKO animals.

For timed matings, noon of the day on which the vaginal plug was first observed was defined as embryonic day 0.5 (E0.5). Mouse foetuses were recovered at E18.5 (just before birth) by Caesarean section. Animals were weaned between 19 and 23 days after birth and deemed adults at 60 days of age. Mice were genotyped by PCR as described previously (Kaufmann *et al*, 2007; Ke *et al*, 2012, 2013). Sequences of primers used for PCR genotyping will be provided upon request.

Mice were kept in microventilated cages (AirLaw) at 21°C and ~ 55% relative humidity on a 14 h light/10 h dark cycle and were fed γ-irradiated breeder cubes (Barastoc, Ridley AgriProducts) and filter-sterilised water adjusted to pH 5.

Histology and microscopy

E18.5 foetuses were euthanised by immediate decapitation following Caesarean section and heads and bodies were placed in Bouin's fixative. Samples were embedded in paraffin and 5-μm coronal serial sections (head) and transverse serial sections (body) were obtained. Slides were stained with haematoxylin and eosin (H&E) and images were photographed using a digital camera (AxioCam HR, Carl Zeiss) on a dissecting microscope (Stemi 2000-C, Carl Zeiss, Germany). For detailed post-mortem examination, E18.5 foetuses were sacrificed by cooling. Dissections were performed using a dissecting microscope (Stemi 2000-C, Carl Zeiss, Germany), and photographs were taken with a digital camera (AxioCam HR, Carl Zeiss).

Quantification and statistical analysis

The ratio of offspring obtained from inter-crosses of $Bok^{-/-}Bax^{+/-}Bak^{-/-}Bid^{-/-}$ and $Bok^{-/-}Bax^{+/-}Bak^{-/-}$ mice at

different stages was analysed by the Chi-square goodness-of-fit test using Stata/SE software16.1 (StataCorp, Texas). Morphometric assessment of tissue area or density was conducted using NIH Image J2 Version 2.3.0/1.53p. Morphometric area data are supplied as raw data (Fig 3) and normalised to the mean body weight per genotype (Fig EV1). Graphs were prepared, and data analysed using GraphPad Prism software 9.0. The statistical tests used are stated in the figure legend. The number of replicates (n) is defined as number of animals and stated in the figures or figure legends.

The number of animals needed to be able to detect changes with statistical significance was determined based on previous studies of a similar nature. Mice were used in order of birth and distributed to experimental groups according to their genotypes. Mice were examined at recovery, at or shortly before birth and before genotyping such that the operator was blinded with respect to the experimental group. No animals or samples were excluded. Where possible, experimental results were obtained by automated methods (e.g. flow cytometry).

Western blot assessment of BID protein levels in cell lines

Lysates of mouse or human cells (DKO, TKO MEFs, RS4;11 or MV4:11 cell lines) or of DKO and TKO cells that had been permeabilised as described below were prepared by resuspending 1×10^6 cells in a volume of 200-μl reducing SDS sample buffer (150 mM Tris pH 6.8, 1.2% (w/v) SDS, 30% (v/v) glycerol, 0.018 mg/ml bromophenol blue, supplemented with 50 μl 2-mercaptoethanol per ml). Recombinant FL-BID protein dilutions (30 nM, 100 nM or 300 nM) were prepared in Sucrose Buffer (100 mM sucrose, 20 mM HEPES-NaOH pH 7.5, 100 mM KCl, 2.5 mM $MgCl_2$, 4 mg/ml Pepstatin A (Sigma-Aldrich, St. Louis, MO, USA) and Complete protease inhibitor cocktail (Roche, Castle Hill, NSW, Australia)), then an equal volume of reducing SDS sample buffer added.

For reducing SDS-PAGE analysis, samples were boiled at 100°C for 5 min before loading 10 μl on 12% TGX gels (BioRad) and resolving at 200 V for 30 min, followed by a wet transfer to PVDF membrane at 30 V for 150 min. Membranes were blotted for BID using rat monoclonal antibody, clone 2D1 (1:1,000; Kaufmann *et al*, 2007) followed by the secondary horseradish peroxidase-conjugated goat anti-rat antibody (3010-05, Southern Biotech, RRID: AB_619911). Horseradish peroxidase was detected with Luminata Forte (WBLUF0500, Millipore, Billerica, MA, USA), and images captured with the ChemiDoc System (Bio-RAD, Hercules, CA, USA).

Cytochrome c release from mitochondria

SV40-transformed mouse embryonic fibroblasts (MEFs) were generated from $Bak^{-/-}Bax^{-/-}$ double knockout (DKO) mice (Willis *et al*, 2007) or $Bok^{-/-}Bax^{-/-}Bak^{-/-}$ triple knockout (TKO) mice (Ke *et al*, 2018). Cells were cultured in Dulbecco's modified Eagle's medium supplemented with 10% (v/v) foetal calf serum, 250 mM L-asparagine and 55 μM 2-mercaptoethanol at 37°C with 10% CO_2. Human BAK was stably expressed in DKO cells with retroviral infection (Dewson *et al*, 2008). Cell lines were confirmed mycoplasma negative.

The human BIM BH3 peptide ([141]DMRPEIWIAQELRRIGDEF-NAYYARR[167], sequence as per (Robin *et al*, 2015)) was purchased from Mimotopes (Notting Hill, VIC, Australia). Full-length human

BID (FL-BID) was produced in-house (WEHI) as described previously (Kluck *et al*, 1999), and caspase-8 cleaved BID (cBID) then generated by incubation with 5 μg/mL recombinant caspase-8 (BD Pharmingen, 556481) for 4 h at 37°C without purification from the caspase-8.

For cytochrome *c* release experiments, 500,000 cells per treatment condition were harvested. Cells were washed in PBS and then resuspended at a concentration of 1×10^7 cells/ml in Sucrose Buffer supplemented with 0.025% w/v digitonin (Calbiochem, Merck, Darmstadt, Germany). Cells were incubated for 10 min on ice to allow the digitonin to permeabilise the cell membrane but leave the mitochondrial membrane intact. The permeabilised cells were then collected by centrifugation at 16,000 *g* for 5 min and the supernatant discarded. Pelleted cells were resuspended in the sucrose buffer and placed on ice before the addition of vehicle, BIM BH3 peptide, cBID or FL-BID. Following treatment additions, cells were moved to 30°C for 30 min and then returned to ice before washing twice with sucrose buffer. Cells were treated with fixation solution (eBioscience) on ice for 30 min, then washed twice with permeabilisation solution (eBioscience). Cells were stained with an antibody against TOM20 (1:500, Santa Cruz sc-11415, rabbit polyclonal) for 30 min on ice and washed once with permeabilisation solution. Next, cells were stained with a rabbit IgG-specific secondary antibody conjugated to AF488 (1:500, Invitrogen #A10034) and an antibody against cytochrome *c* conjugated to APC (1:50, clone REA702, cat. no. 130-111-368; Miltenyi Biotec) and washed once with permeabilisation solution. Cells were assessed by flow cytometry (LSR Fortessa x20, BD Biosciences) and analysed using FlowJo 10.8.1 (BD Biosciences). Cells were gated for TOM20 positivity (1D, histogram) to exclude cells that were incompletely permeabilised. Histograms for TOM20 staining (TOM20-positive only) and cytochrome *c* staining (cytochrome *c* gated on TOM20-positive cells) were generated using FlowJo 10.8.1 (BD Biosciences). Median fluorescence intensity (MFI) was plotted for duplicate experiments with Prism 9 (GraphPad LLC).

Data availability

This study includes no data that would need to be deposited in external repositories.

Expanded View for this article is available online.

Author contributions

Andreas Strasser: Conceptualization; resources; formal analysis; supervision; funding acquisition; project administration. **Francine S Ke:** Conceptualization; data curation; formal analysis; validation; investigation; methodology; project administration. **Steven Holloway:** Investigation; methodology. **Melissa H Little:** Conceptualization. **Anne K Voss:** Conceptualization; data curation; formal analysis; investigation; visualization; methodology; project administration. **Ruth M Kluck:** Formal analysis; investigation. **Rachel T Uren:** Data curation; formal analysis; investigation. **Agnes W Wong:** Data curation; formal analysis; investigation.

In addition to the CRediT author contributions listed above, the contributions in detail are:

FSK, RMK, AS and AKV designed study, interpreted results and wrote the manuscript. FSK conducted experiments with help from AKV. MHL and SH helped with the analysis of the kidney phenotype. RTU and AWW conducted the biochemical analysis of the effects of BID.

Disclosure and competing interest statement

The authors declare that they have no conflict of interest.

References

Arya R, White K (2015) Cell death in development: signaling pathways and core mechanisms. *Semin Cell Dev Biol* 39: 12–19

Basson MA, Akbulut S, Watson-Johnson J, Simon R, Carroll TJ, Shakya R, Gross I, Martin GR, Lufkin T, McMahon AP *et al* (2005) Sprouty1 is a critical regulator of GDNF/RET-mediated kidney induction. *Dev Cell* 8: 229–239

Basson MA, Watson-Johnson J, Shakya R, Akbulut S, Hyink D, Costantini FD, Wilson PD, Mason IJ, Licht JD (2006) Branching morphogenesis of the ureteric epithelium during kidney development is coordinated by the opposing functions of GDNF and Sprouty1. *Dev Biol* 299: 466–477

Batourina E, Tsai S, Lambert S, Sprenkle P, Viana R, Dutta S, Hensle T, Wang F, Niederreither K, McMahon AP *et al* (2005) Apoptosis induced by vitamin a signaling is crucial for connecting the ureters to the bladder. *Nat Genet* 37: 1082–1089

Billen LP, Shamas-Din A, Andrews DW (2008) Bid: a Bax-like BH3 protein. *Oncogene* 27: S93–S104

Bingham C, Bulman MP, Ellard S, Allen LI, Lipkin GW, Hoff WG, Woolf AS, Rizzoni G, Novelli G, Nicholls AJ *et al* (2001) Mutations in the hepatocyte nuclear factor-1beta gene are associated with familial hypoplastic glomerulocystic kidney disease. *Am J Hum Genet* 68: 219–224

Bolar NA, Golzio C, Živná M, Hayot G, Van Hemelrijk C, Schepers D, Vandeweyer G, Hoischen A, Huyghe JR, Raes A *et al* (2016) Heterozygous loss-of-function SEC61A1 mutations cause autosomal-dominant Tubulo-interstitial and glomerulocystic kidney disease with anemia. *Am J Hum Genet* 99: 174–187

Bouillet P, Cory S, Zhang LC, Strasser A, Adams JM (2001) Degenerative disorders caused by Bcl-2 deficiency prevented by loss of its BH3-only antagonist Bim. *Dev Cell* 1: 645–653

Chou JJ, Li H, Salvesen GS, Yuan J, Wagner G (1999) Solution structure of BID, an intracellular amplifier of apoptotic signaling. *Cell* 96: 615–624

Czabotar PE, Lessene G, Strasser A, Adams JM (2014) Control of apoptosis by the BCL-2 protein family: implications for physiology and therapy. *Nat Rev Mol Cell Biol* 15: 49–63

Dewson G, Kratina T, Sim HW, Puthalakath H, Adams JM, Colman PM, Kluck RM (2008) To trigger apoptosis, Bak exposes its BH3 domain and homodimerizes its BH3:Groove interactions. *Mol Cell* 30: 369–380

Diez-Roux G, Banfi S, Sultan M, Geffers L, Anand S, Rozado D, Magen A, Canidio E, Pagani M, Peluso I *et al* (2011) A high-resolution anatomical atlas of the transcriptome in the mouse embryo. *PLoS Biol* 9: e1000582

Dressler GR (2009) Advances in early kidney specification, development and patterning. *Development* 136: 3863–3874

Eskes R, Desagher S, Antonsson B, Martinou JC (2000) Bid induces the oligomerization and insertion of Bax into the outer mitochondrial membrane. *Mol Cell Biol* 20: 929–935

Flores-Romero H, Hohorst L, John M, Albert MC, King LE, Beckmann L, Szabo T, Hertlein V, Luo X, Villunger A *et al* (2022) BCL-2-family protein tBID can act as a BAX-like effector of apoptosis. *EMBO J* 41: e108690

García-Sáez AJ, Mingarro I, Pérez-Payá E, Salgado J (2004) Membrane-insertion fragments of Bcl-xL, Bax, and bid. *Biochemistry* 43: 10930–10943

Georgas KM, Armstrong J, Keast JR, Larkins CE, McHugh KM, Southard-Smith EM, Cohn MJ, Batourina E, Dan H, Schneider K *et al* (2015) An illustrated anatomical ontology of the developing mouse lower urogenital tract. *Development* 142: 1893–1908

Glucksmann A (1951) Cell deaths in normal vertebrate ontogeny. *Biol Rev Camb Philos Soc* 26: 59–86

Ito M, Yoshioka M (1999) Regression of the hyaloid vessels and pupillary membrane of the mouse. *Anat Embryol* 200: 403–411

Jost PJ, Grabow S, Gray D, McKenzie MD, Nachbur U, Huang DC, Bouillet P, Thomas HE, Borner C, Silke J *et al* (2009) XIAP discriminates between type I and type II FAS-induced apoptosis. *Nature* 460: 1035–1039

Kamada S, Shimono A, Shinto Y, Tsujimura T, Takahashi T, Noda T, Kitamura Y, Kondoh H, Tsujimoto Y (1995) Bcl-2 deficiency in mice leads to pleiotropic abnormalities: accelerated lymphoid cell death in thymus and spleen, polycystic kidney, hair hypopigmentation, and distorted small intestine. *Cancer Res* 55: 354–359

Kaufmann T, Strasser A, Jost PJ (2012) Fas death receptor signalling: roles of bid and XIAP. *Cell Death Differ* 19: 42–50

Kaufmann T, Tai L, Ekert PG, Huang DC, Norris F, Lindemann RK, Johnstone RW, Dixit VM, Strasser A (2007) The BH3-only protein bid is dispensable for DNA damage- and replicative stress-induced apoptosis or cell-cycle arrest. *Cell* 129: 423–433

Ke F, Bouillet P, Kaufmann T, Strasser A, Kerr J, Voss AK (2013) Consequences of the combined loss of BOK and BAK or BOK and BAX. *Cell Death Dis* 4: e650

Ke F, Voss A, Kerr JB, O'Reilly LA, Tai L, Echeverry N, Bouillet P, Strasser A, Kaufmann T (2012) BCL-2 family member BOK is widely expressed but its loss has only minimal impact in mice. *Cell Death Differ* 19: 915–925

Ke FFS, Vanyai HK, Cowan AD, Delbridge ARD, Whitehead L, Grabow S, Czabotar PE, Voss AK, Strasser A (2018) Embryogenesis and adult life in the absence of intrinsic apoptosis effectors BAX, BAK, and BOK. *Cell* 173: e1217

Kim J, Lee GS, Tisher CC, Madsen KM (1996) Role of apoptosis in development of the ascending thin limb of the loop of Henle in rat kidney. *Am J Phys* 271: F831–F845

Kluck RM, Esposti MD, Perkins G, Renken C, Kuwana T, Bossy-Wetzel E, Goldberg M, Allen T, Barber MJ, Green DR *et al* (1999) The pro-apoptotic proteins, bid and Bax, cause a limited permeabilization of the mitochondrial outer membrane that is enhanced by cytosol. *J Cell Biol* 147: 809–822

Koseki C, Herzlinger D, al-Awqati Q (1992) Apoptosis in metanephric development. *J Cell Biol* 119: 1327–1333

Kreidberg JA, Sariola H, Loring JM, Maeda M, Pelletier J, Housman D, Jaenisch R (1993) WT-1 is required for early kidney development. *Cell* 74: 679–691

Li H, Zhu H, Xu CJ, Yuan J (1998) Cleavage of BID by caspase 8 mediates the mitochondrial damage in the Fas pathway of apoptosis. *Cell* 94: 491–501

Lindsten T, Ross AJ, King A, Zong WX, Rathmell JC, Shiels HA, Ulrich E, Waymire KG, Mahar P, Frauwirth K *et al* (2000) The combined functions of proapoptotic Bcl-2 family members bak and bax are essential for normal development of multiple tissues. *Mol Cell* 6: 1389–1399

Little MH, McMahon AP (2012) Mammalian kidney development: principles, progress, and projections. *Cold Spring Harb Perspect Biol* 4: a008300

Luo X, Budihardjo I, Zou H, Slaughter C, Wang X (1998) Bid, a Bcl2 interacting protein, mediates cytochrome c release from mitochondria in response to activation of cell surface death receptors. *Cell* 94: 481–490

Muchmore SW, Sattler M, Liang H, Meadows RP, Harlan JE, Yoon HS, Nettesheim D, Chang BS, Thompson CB, Wong SL *et al* (1996) X-ray and NMR structure of human Bcl-xL, an inhibitor of programmed cell death. *Nature* 381: 335–341

Nakayama K, Nakayama K, Negishi I, Kuida K, Sawa H, Loh DY (1994) Targeted disruption of Bcl-2 alpha beta in mice: occurrence of gray hair, polycystic kidney disease, and lymphocytopenia. *Proc Natl Acad Sci USA* 91: 3700–3704

Nishinakamura R, Matsumoto Y, Nakao K, Nakamura K, Sato A, Copeland NG, Gilbert DJ, Jenkins NA, Scully S, Lacey DL *et al* (2001) Murine homolog of SALL1 is essential for ureteric bud invasion in kidney development. *Development* 128: 3105–3115

Ranger AM, Malynn BA, Korsmeyer SJ (2001) Mouse models of cell death. *Nat Genet* 28: 113–118

Ren D, Tu HC, Kim H, Wang GX, Bean GR, Takeuchi O, Jeffers JR, Zambetti GP, Hsieh JJ, Cheng EH (2010) BID, BIM, and PUMA are essential for activation of the BAX- and BAK-dependent cell death program. *Science* 330: 1390–1393

Robin AY, Krishna Kumar K, Westphal D, Wardak AZ, Thompson GV, Dewson G, Colman PM, Czabotar PE (2015) Crystal structure of Bax bound to the BH3 peptide of Bim identifies important contacts for interaction. *Cell Death Dis* 6: e1809

Sánchez MP, Silos-Santiago I, Frisén J, He B, Lira SA, Barbacid M (1996) Renal agenesis and the absence of enteric neurons in mice lacking GDNF. *Nature* 382: 70–73

Sasaki C, Yamaguchi K, Akita K (2004) Spatiotemporal distribution of apoptosis during normal cloacal development in mice. *Anat Rec A Discov Mol Cell Evol Biol* 279: 761–767

Scaffidi C, Fulda S, Srinivasan A, Friesen C, Li F, Tomaselli KJ, Debatin KM, Krammer PH, Peter ME (1998) Two CD95 (APO-1/Fas) signaling pathways. *EMBO J* 17: 1675–1687

Singh R, Letai A, Sarosiek K (2019) Regulation of apoptosis in health and disease: The balancing act of BCL-2 family proteins. *Nat Rev Mol Cell Biol* 20: 175–193

Smith P, Dunn M (1979) Duplication of the upper urinary tract. *Ann R Coll Surg Engl* 61: 281–286

Sorenson CM, Rogers SA, Korsmeyer SJ, Hammerman MR (1995) Fulminant metanephric apoptosis and abnormal kidney development in bcl-2-deficient mice. *Am J Phys* 268: F73–F81

Strasser A, Jost PJ, Nagata S (2009) The many roles of FAS receptor signaling in the immune system. *Immunity* 30: 180–192

Suzuki M, Youle RJ, Tjandra N (2000) Structure of Bax: coregulation of dimer formation and intracellular localization. *Cell* 103: 645–654

Taniguchi H, Kitaoka T, Gong H, Amemiya T (1999) Apoptosis of the hyaloid artery in the rat eye. *Ann Anat* 181: 555–560

Vaux DL, Korsmeyer SJ (1999) Cell death in development. *Cell* 96: 245–254

Veis DJ, Sorenson CM, Shutter JR, Korsmeyer SJ (1993) Bcl-2-deficient mice demonstrate fulminant lymphoid apoptosis, polycystic kidneys, and hypopigmented hair. *Cell* 75: 229–240

Voss AK, Strasser A (2020) The essentials of developmental apoptosis. *F1000Res* 9: F1000 Faculty Rev-148

Wainwright EN, Wilhelm D, Combes AN, Little MH, Koopman P (2015) ROBO2 restricts the nephrogenic field and regulates Wolffian duct-nephrogenic cord separation. *Dev Biol* 404: 88−102

Wang K, Yin XM, Chao DT, Milliman CL, Korsmeyer SJ (1996) BID: a novel BH3 domain-only death agonist. *Genes Dev* 10: 2859−2869

Willis SN, Fletcher JI, Kaufmann T, van Delft MF, Chen L, Czabotar PE, Ierino H, Lee EF, Fairlie WD, Bouillet P *et al* (2007) Apoptosis initiated when BH3 ligands engage multiple Bcl-2 homologs, not Bax or Bak. *Science* 315: 856−859

Xu PX, Adams J, Peters H, Brown MC, Heaney S, Maas R (1999) Eya1-deficient mice lack ears and kidneys and show abnormal apoptosis of organ primordia. *Nat Genet* 23: 113−117

Yin XM, Wang K, Gross A, Zhao Y, Zinkel S, Klocke B, Roth KA, Korsmeyer SJ (1999) Bid-deficient mice are resistant to Fas-induced hepatocellular apoptosis. *Nature* 400: 886−891

Youle RJ, Strasser A (2008) The BCL-2 protein family: opposing activities that mediate cell death. *Nat Rev Mol Cell Biol* 9: 47−59

Zha J, Weiler S, Oh KJ, Wei MC, Korsmeyer SJ (2000) Posttranslational N-myristoylation of BID as a molecular switch for targeting mitochondria and apoptosis. *Science* 290: 1761−1765